Antiparasitic effect *in vitro*, activity in a murine model of Chagas disease, and structural characterization in complex with the target enzyme CYP51 from *Trypanosoma cruzi* of the potent clinical candidate VT-1161

William J. Hoekstra[a], Tatiana Y. Hargrove[b], Zdzislaw Wawrzak[c], Denis D.G. Batista[d], Cristiane F. da Silva[d], Aline SG Nefertiti[d], Girish Rachakonda[e], Robert J. Schotzinger[a], Fernando Villalta[e], Maria de Nazaré C. Soeiro[d], Galina I. Lepesheva[b,f,] *

Viamet Pharmaceuticals, Inc., Durham, North Carolina, USA[a]; Department of Biochemistry Vanderbilt University School of Medicine, Nashville, Tennessee, USA[b]; Synchrotron Research Center, Life Science Collaborative Access Team, Northwestern University, Argonne, Illinois, USA[c]; Laboratório de Biologia Celular, Instituto Oswaldo Cruz, Fundação Oswaldo Cruz, Rio de Janeiro, RJ, Brazil[d]; Department of Microbiology and Immunology, Meharry Medical College, Nashville, Tennessee, USA[e]; Center for Structural Biology Vanderbilt University, Nashville, Tennessee, USA[f]

* Address correspondence to Galina Lepesheva, galina.i.lepesheva@vanderbilt.edu

Running title: VT-1161 as a therapeutic agent for Chagas disease

Abstract

A novel antifungal drug candidate, 1-tetrazole VT-1161 [(R)-2-(2,4-difluorophenyl)-1,1-difluoro-3-(1H-tetrazol-1-yl)-1-(5-(4-(2,2,2-trifluoroethoxy)phenyl)pyridin-2-yl)propan-2-ol], which is currently in two Phase 2b antifungal clinical trials, was found to be a tight-binding ligand (the apparent dissociation constant (K_d) = 24 nM) and a potent inhibitor of cytochrome P450 sterol 14α-demethylase (CYP51) from the protozoan pathogen *Trypanosoma cruzi*. Moreover, VT-1161 revealed high antiparasitic efficiency in cellular experiments against amastigotes of the Tulahuen strain of *T. cruzi* (EC_{50}=2.5 nM) and was active *in vivo*, causing >99.8% of peak parasitemia suppression in a mouse model of infection with the naturally drug-resistant Y strain of the parasite. The data strongly support the potential utility of VT-1161 in the treatment of Chagas disease. Structural characterization of *T. cruzi* CYP51 in complex with VT-1161 provides insights into the molecular basis for the compound inhibitory potency and paves the way for further rational development of this novel, tetrazole-based inhibitory chemotype, both for antiprotozoan, and for antifungal chemotherapy.

Keywords: Chagas disease, *Trypanosoma cruzi*, VT-1161, sterol 14α-demethylase (CYP51), inhibition, X-ray structure, structure-based drug design

INTRODUCTION

Chagas disease is a vector-borne zoonosis, caused by a genetically diverse population of the protozoan parasite *Trypanosoma cruzi* (1, 2). The infection is transmitted to more than 150 mammalian species by triatominae insects, often called "kissing bugs". The other most frequent ways of transmission to humans involve: blood transfusion, organ transplantation, oral ingestion via contaminated food or drinks, and from mother to child. The disease is endemic in Central and South America. With human migration and HIV co-infections, Chagas also is now found in all other parts of the globe. According to the World Health Organization, worldwide, an estimated 6-8 million people are infected with *Trypanosoma cruzi*, with 24,000 fatalities each year (3). The situation is becoming particularly alarming in North America, due to the broadening of the area of vector habitat (4) and, accordingly, the wide spread of the naturally infected wild animals that form the disease reservoir (5). Some estimates indicate that there are up to one million cases of Chagas disease in the US, most of them remaining undetected (6-9). Kissing bug bites have been reported in 43 states of the US.

In the meantime, Chagas disease remains essentially incurable, with two nitro-heterocyclic compounds, benznidazole and nifurtimox, being the only drugs on the market and available in Latin America. The mechanism of their action is not completely clear, though it is believed to involve oxidative stress via the formation of free radicals and electrophilic metabolites that are generated when the nitro-heterocyclic group of the compounds undergoes nitroreductase-mediaded activation (10-12). Due to their quite serious toxicity and insufficient efficiency (13), benznidazole and nifurtimox are not approved by the US Food and Drug Administration (FDA), and therefore they are not prescribed there. Although it was reported that these drugs can potentially be obtained by special request from the

66 Center for Disease Control (8), http://www.cdc.gov/parasites/chagas/health_professionals/tx.html),
67 to our knowledge, most physicians are unaware of such opportunity.

68 There has been hope that repurposing of two antifungal drugs (posaconazole and ravuconazole)
69 may resolve the problem (4, 14), though thus far the results of their clinical trials for Chagas disease
70 have been quite controversial (~ 80% treatment failure and quite expressed side effects (15, 16)).
71 Both posaconazole and ravuconazole are 1-(1,2,4-triazole) based inhibitors of fungal sterol 14α-
72 demethylase (CYP51), the cytochrome P450 enzyme essential for the production of sterols, which
73 are required for the formation of viable fungal membranes (17). Similar to fungi, *T. cruzi* is
74 completely dependent on the endogenously synthesized sterols (18). However, because *T. cruzi* is an
75 intracellular parasite and has a complex life cycle involving so called quiescent (dormant) forms
76 with reduced metabolic activity (15, 19), it is reasonable to presume that alternative CYP51
77 inhibitors, with optimized pharmacological properties (e.g. higher bioavailability and cellular
78 permeability, broader tissue distribution, lower toxicity) and particularly with the lower production
79 costs, which would easily afford longer treatment periods, should be seriously considered as
80 potential antichagasic agents.

81 Herein, we characterized as a *T. cruzi* CYP51 ligand and inhibitor the novel 1-tetrazole based
82 Phase 2b antifungal clinical agent VT-1161 (20). As we reported previously, this low-affinity metal
83 binding group-bearing agent displays high target-selectivity (weak inhibitory effect on human drug-
84 metabolizing cytochromes P450) (21, 22) and excellent oral activity (23). With this new drug
85 candidate, orally-administered therapy targets recurrent vulvovaginal candidiasis and
86 onychomycosis. The initial antifungal program focused on yeasts and dermatophytes, resulting
87 ultimately in the selection of VT-1161 for clinical Phase 1 pharmacokinetic and Phase 2a efficacy
88 studies. The safety and pharmacokinetics in humans have mirrored the preclinical animal data as

89 insofar VT-1161 appeared to raise no safety concerns and achieved an excellent oral PK profile
90 exhibiting an extended half-life (23-25). All data to date support the potential for VT-1161 as a best-
91 in-class CYP51 antifungal, overcoming the side-effect profiles of marketed fungal CYP51 inhibitors
92 (26) that offer limited dosing options. The results of this study indicate the noteworthy anti-*T. cruzi*
93 potency of VT-1161.
94
95 **MATERIALS AND METHODS**
96 **Proteins.** All protein genes were His-tag-engineered at the C-terminus, subcloned into the
97 pCW expression vector and expressed in the *E. coli* strain HMS174(DE3) (Novagen). For
98 enzymatic assays, including ligand binding and reconstitution of sterol 14α-demethylase activity
99 *in vitro*, we used the full-length Tulahuen *T. cruzi* CYP51 (GenBank IDs AY856083) (27). The
100 enzyme was purified by affinity chromatography on Ni^{2+}-nitrotriloacetate agarose (Qiagen)
101 followed by cation exchange chromatography on carboxymethyl Sepharose Fast Flow (GE
102 Healthcare) (27). The samples of CYP51 enzymes from *Aspergillus fumigatus* and *Candida*
103 *albicans* were expressed and purified as previously described (28, 29). The CYP51 electron
104 donor partner, NADPH-cytochrome P450 reductase (CPR), was from *T. brucei* and rat, for
105 protozoan and fungal orthologs, respectively (29-31). For crystallographic experiments, the *T.*
106 *cruzi* CYP51 was truncated to replace the 30-amino acid membrane anchor sequence at the N-
107 terminus (up to P31) with the more polar 5-amino acid sequence fragment MAKKT- (32) and
108 purified in three steps, including anion exchange chromatography on DEAE-Sepharose (GE
109 Healthcare), affinity chromatography on Ni^{2+}-NTA agarose, and cation exchange
110 chromatography on CM-Sepharose Fast Flow. Complexes with VT-1161 were obtained by
111 saturating the protein with the inhibitor during the last step of purification (33) by adding a 20

112 mM stock solution of VT-1161 in dimethyl sulfoxide (DMSO) to the washing and elution
113 buffers, with a final concentration of 10 µM.

114 **Spectroscopic measurements and ligand binding assay.** UV-visible absorption spectra
115 were recorded using a dual-beam Shimadzu UV-2401PC spectrophotometer in 50 mM potassium
116 phosphate buffer (pH 7.2) containing 10% glycerol (v/v). P450 concentrations were estimated
117 from the Soret band intensity using ε_{417} 117 mM^{-1} cm^{-1} (27) or $\Delta\varepsilon_{450\text{-}490}$ 91 mM^{-1} cm^{-1} for the
118 reduced carbon monoxide difference spectra (34). Titrations with VT-1161 were carried out at
119 0.3 μM P450 concentration in 5-cm optical path length cuvettes, with ligand binding being
120 monitored as a 'Type II' spectral response that reflects coordination of a basic heterocyclic
121 nitrogen to the P450 heme iron (red shift in the Soret band maximum from 417 to 421-427 nm
122 (35) depending on the basicity of the coordinating nitrogen (33)). Difference spectra were
123 generated by recording the P450 absorbance in a sample cuvette versus the absorbance in a
124 reference cuvette, both containing the same amount of the protein. Aliquots of VT-1161
125 dissolved in DMSO were added to the sample cuvette in the concentration range 0.1 - 1.0 μM,
126 with each titration step being 0.1 μM. At each step, the corresponding volume of DMSO was
127 added to the reference cuvette. The apparent dissociation constants of the CYP51-VT-1161
128 complex (K_d) were calculated in GraphPad Prism 6 software (GraphPad, La Jolla, CA) by fitting
129 the data for the ligand-induced absorbance changes in the difference spectra $\Delta(A_{max}\text{-}A_{min})$ versus
130 ligand concentration to the quadratic equation 1 (tight-binding ligands, (33)),

131 $$\Delta A=(\Delta A_{max}/2E)((L+E+K_d)-((L+E+K_d)^2-4LE)^{0.5}) \quad \text{(Eq.1)}$$

132 where [L] and [E] are the total concentrations of ligand and enzyme used for the titration,
133 respectively.

Reconstitution of catalytic activity and CYP51 inhibition assay. Enzymatic activity of *T. cruzi* CYP51 was reconstituted *in vitro* as described previously using eburicol (24-methylenedihydrolanosterol) as the substrate (27). Briefly, the reaction mixture contained 1 µM CYP51, 2 µM CPR, 100 µM dilauroyl-α-phosphatidylcholine, 0.4 mg/mL isocytrate dehydrogenase and 25 mM sodium isocitrate in 20 mM MOPS (pH 7.4), 50 mM KCl, 5 mM $MgCl_2$ and 10% glycerol. After addition of the [^{3}H]-radiolabeled sterol substrate (~2,000 cpm/nmol, final concentration 50 µM) the mixture was preincubated for 5 min at 37 ºC; the reaction was initiated by addition of 100 µM NADPH and stopped by extraction of the sterols with ethyl acetate. Enzymatic activities of CYP51 orthologs from *C. albicans* (30) and *A. fumigatus* (29) were reconstituted with eburicol and lanosterol, respectively. The extracted sterols were dried, dissolved in methanol, and analyzed by a reverse-phase HPLC system (Waters) equipped with *β*-RAM detector (INUS Systems, Inc.) using a Nova Pak C18 column and a linear gradient H_2O:CH_3CN:CH_3OH (1.0:4.5:4.5, v/v/v) (solvent A) to CH_3OH (solvent B), increasing from 0 to 100% B for 30 min at a flow rate of 1.0 ml/min. The inhibitory potencies of VT-1161 on CYP51 activity were compared on the basis of decreases in substrate conversion in 60 min reactions (31-33) at a molar ratio of substrate/enzyme/inhibitor of 50/1/2 (33, 36).

***T. cruzi* cellular growth inhibition assay.** Cellular *T. cruzi* infection assay was performed using the highly invasive 20A clone of the Tulahuen strain of the parasite (37). *T. cruzi* trypomastigotes expressing green fluorescent protein (GFP) were generated as described (32). Trypomastigotes were used to infect cardiomyocyte monolayers in 48-well tissue culture plates and in 8-well LabTech tissue culture chambers in triplicate at the ratio of 10 parasites per cell as described (38, 39). Cultures were incubated with DMEM supplemented with 10% fetal bovine

serum (FBS) as described (38). Unbound trypomastigotes were removed by washing the cellular monolayers with DMEM; and infected monolayers were exposed to several concentrations of VT-1161 (from 1 to 500 nM), dissolved in DMSO/DMEM free of phenol red in triplicate at 24 h of infection and co-cultured in DMEM + 10% FBS for 48 h to observe parasite multiplication. 72 h after infection, the cardiomyocyte monolayers were washed with phosphate-buffered saline, and the infection was fluorimetically quantified as Relative Fluorescence Units (RFU) using a Synergy HT fluorometer (Biotek Instruments) (39). For fluorescence microscopy observation, the infection assays were performed in 8-well LabTech tissue culture chambers in triplicate. 72 h after infection the cardiomyocyte monolayers were fixed with 2.5% paraformaldehyde and stained with 4′,6-diamidino-2-phenylindole, to visualize DNA, and with Alexa fluor 546 phalloidin (Invitrogen), to visualize cardiomyocyte actin myofibrils (38).

Efficacy *in vivo* assay. Female Swiss mice (18-20 g) were obtained from the animal facilities of the Oswaldo Cruz Foundation (CECAL, Rio de Janeiro, Brazil). Mice were housed at six per cage and kept in a conventional room at 20-24°C under a 12/12 h light/dark cycle. The animals were provided with sterilized water and food *ad libitum*. All procedures and experimental protocols were conducted in accordance with the guidelines issued by the FIOCRUZ Committee of Ethics for the Use of Animals (CEUA LW16/14). Animals were inoculated with 10^4 trypomastigotes of the Y strain of *T. cruzi* by intraperitoneal (ip) injection. Three experimental groups were established: (i) 6 mice treated with VT-1161 at 50 mg/kg once a day, (ii) 6 mice treated with 0.5 % carboxymethylcellulose (vehicle), and (iii) 6 mice maintained as infected and untreated control. VT-1161 was suspended in 0.5% (w/v) carboxymethylcellulose, and each treated animal received 0.2 ml of drug suspension by gavage. The treatment was started at 5 days postinfection (p.i.) that corresponds to parasitemia onset at this experimental mouse model and

lasted up to 9 dpi (five consecutive daily doses) to cover the peak of parasitemia for the Y strain infection (day 8 p.i.). Parasitemia was evaluated by microscopic examination of fresh blood samples (direct microscopic counting of parasites in 5 µL of tail blood) and performed on days 4, to select only the animals that revealed observable parasitemia, and then on days 7 and 8.

X-ray crystallography. The initial screening of crystallization conditions was carried out using Hampton Research crystallization kits. The crystals were obtained by the hanging drop vapor diffusion method at 18ºC. Equal volumes of 300 µM *T. cruzi* CYP51-VT-1161 complex in 20 mM K-phosphate buffer, pH 7.2, containing 100 mM NaCl, 0.1 mM EDTA, 10% glycerol, 5.8 mM *tris*(carboxyethyl)phosphine (TCEP), and 0.048 mM n-tridecyl-beta-d-maltoside were mixed with mother liquor (0.2 M lithium sulfate, 0.1 M HEPES (pH 7.4), and 25% polyethylene glycol 3,350 (w/v) and equilibrated against the reservoir solution. Crystals appeared after several days and were cryoprotected by plunging them into a drop of reservoir solution supplemented with 40% glycerol (v/v), flash-cooled in liquid nitrogen and then prescreened on Bruker Microstar microfocus rotating-anode X-ray generator/Proteum PT135 CCD area detectors. Crystals that diffracted to ~3.0 Å resolution were subsequently used for the data collection. The data were collected on the 21-ID-F beamline of the Life Sciences Collaborative Access Team (LS-CAT) at the Advanced Photon Source, Argonne National Laboratory (Argonne, IL) at 100 K, a wavelength of 0.9786 Å, and using a MAR225 CCD detector. The diffraction images were integrated using Mosflm and scaled with Aimless (CCP4 Program Suite 6.3.0 (40)) in the trigonal P3(1)21 space group to maximum resolutions of 2.75 Å. Solvent content was estimated with the Matthews probability calculator (40). The crystal structure was determined by molecular replacement in PhaserMR using the atomic coordinates of posaconazole-bound *T. cruzi* CYP51 structure (PDB code 3K1O) as the search model. An iterative model of the protein-inhibitor

complex was then built with Coot (41) and refined with Refmac5 in CCP4 suite (40). Data collection and refinement statistics are shown in Table 1. The atomic coordinates and structure factors have been deposited in the Protein Data Bank under ID code 5JAR. The ID-codes of other *T. cruzi* CYP51 structures discussed in this work are 3K1O (complex with the antifungal drug triazole posaconazole (32)), 4CK8 (complex with the experimental imidazole derivative LFD (36)), and 3ZG2 (complex with the fenarimol derivative pyridine UDO (33)). Structure superimpositions were done in LSQkab of the CCP4 suite. Molecular volumes and surface areas were calculated in Accelrys Discovery Studio Visualizer 2.5 (probe radius 1.4 Å). Figures were prepared with Pymol and Chimera.

RESULTS

Characterization of VT-1161 as a *T. cruzi* CYP51 heme-coordinating ligand. Titration of *T. cruzi* CYP51 with VT-1161 caused a red shift in the Soret band absorbance, which in the difference spectra was expressed as the peak, the trough, and the isosbestic point at 423, 386, and 408 nm, respectively (Figure 1A), indicating expulsion of a water molecule from the cytochrome P450 active site and coordination of a basic nitrogen atom of the ligand to the heme iron. Although the shape of the Type II spectral response (35) suggested that the length of the N-Fe coordination bond in the enzyme-ligand complex is likely to be relatively longer than it is usually observed in the CYP51 complexes with imidazole (2.0-2.04 Å, the peak at 428 nm), or triazole (2.07-2.15 Å, the peak at 426 nm) based ligands (33), the apparent binding affinity of VT-1161 was rather high, with the calculated spectral dissociation constant (K_d) being in the lower nanomolar range (24 nM), the value comparable with that obtained upon spectral titration

of *C. albicans* CYP51 (21 nM) and about twice lower than the K_d calculated for CYP51 from A. fumigatus (47 nM) (Figure 1B).

VT-1161 as an inhibitor of enzymatic activity of sterol 14α-demethylase. At a two fold molar excess over the enzyme, VT-1161 inhibited 94% of the substrate conversion by *T. cruzi* CYP51 (Figure 2), thus, showing the inhibitory effect comparable with its effect on the activity of CYP51 from *C. albicans* (affording 2.5% of substrate conversion) and somewhat stronger than the effect on the activity CYP51B from *A. fumigatus* (17% of substrate conversion). The results correlate with the higher activity of VT-1161 against yeast than against filamentous fungi and implied that the compound can potentially serve as a promising antichagasic agent.

Antiparasitic effect of VT-1161 in *T. cruzi* cells. Cellular experiments were preformed using the highly invasive 20A clone of the Tulahuen strain of *T. cruzi* because it infects >98% of exposed cardiomyocytes (37) (Figure 3A). The antiparasitic activity of VT-1161 was analysed in the clinically most relevant form of the parasite, intracellular amastigotes, by quantifying the rate of their replication within the infected cardiomyocytes (examples are shown in Figure 3 B, C). The obtained dose-response curve (Figure 3D) indicates that the effect of the drug is already seen at 1 nM concentration. The EC_{50} value (the compound concentration capable of reducing the infection by 50% as compared with nontreated infected controls) was achieved at ~2.5 nM VT-1161, which is comparable with the anti-Tulahuen *T. cruzi* activity reported for one of the most potent sterol biosynthetic inhibitors, posaconazole (EC_{50} = 1 nM (15)),. and is about three orders of magnitude lower that the EC_{50} value determined for benznidazole (2.4 μM) (12). At the concentration of 200 nM VT-1161 kills all parasites within cardiomyocytes. The same effect is seen at 500 nM (data not shown). Thus, VT-1161 has demonstrated significant efficiency against *T. cruzi* and therefore was further tested in *in vivo* experiments.

248 **Activity of VT-1161 in the murine model of *T. cruzi* infection.** In these short-term *in vivo*
249 experiments we evaluated the ability of VT-1161 to suppress parasitemia in the acute infection of
250 mice with the Y strain of *T. cruzi*, because the Y strain is known to be naturally moderately
251 resistant to nitroderivatives, such as benznidazole and nifurtimox (1) and have decreased
252 susceptibility to the CYP51 inhibitors posaconazole (42, 43) and VNI (44). Besides, infection of
253 Swiss mice using 10^4 bloodstream forms of the Y strain *T. cruzi* reaches its peak of parasitemia
254 on day 8 (44), which allows for a relatively fast selection of potentially promising compounds.
255 Although the treatment with VT-1161 was started on day 5 (corresponding to the onset of
256 parasitemia), after two days of the drug administration the infection was restrained to 2.3%
257 relative to the control group of mice, while a three-day treatment with VT-1161 caused >99.8%
258 suppression of parasitemia (Figure 4). After a five-day treatment period all treated mice survived
259 (not shown).

260 **X-ray co-structure of *T. cruzi* CYP51-VT-1161 complex.** In order to better understand VT-
261 1161 potency and selectivity, we determined the X-ray co-structure of its complex with *T. cruzi*
262 CYP51. The complex has one monomer in the asymmetric unit. The protein chain is seen from
263 Lys-29 (KKT**P**- in the N-terminal MAKKT**P**- sequence) to Lys-478 (the fifth residue from the
264 C-terminus), and one residue (Pro-222, G''G loop) is missing. The electron density for VT-1161
265 is well defined, showing single orientation of the inhibitor molecule within the enzyme substrate
266 binding cavity and full occupancy. The 2Fo-Fc electron density map weighted at 1.3 σ is shown
267 in Figure 5A, the structural formula of VT-1161 in the same orientation is given above.

268 In the *T. cruzi* CYP51 active site the molecule of VT-1161 (ligand PDB ID VT1, molecular
269 weight 527, log P=5.07) occupies the volume of 572 $Å^3$, with the surface area being 439 A^2. The
270 tetrazole ring binds to the CYP51 heme iron via the N4 nitrogen, which forms the sixth axial

(distal) coordination bond, the sulfur atom of C422 serving as the canonical P450 fifth axial (proximal) ligand (Figure 5B). The length of the N4-Fe coordination bond is 2.2 Å, which is in good agreement with the shape of the Type II spectral response and reflects moderate basicity of the N4-tetrazole nitrogen (between that of N4 in triazoles (the corresponding bond length 2.07-2.15 Å) and N1 in pyridines (2.30-2.35 Å) (33, 45) thus providing the molecular background for the high selectivity of this compound to CYP51 and its weak inhibitory effect on human drug metabolizing cytochromes P450 (21).

At the distance of 5 Å, VT-1161 is contacted by 19 amino acid residues of *T. cruzi* CYP51 (Figure 5B). Of these residues, five (F48, P210, V213, F214, and M460) form the entry into the CYP51 substrate access channel, possibly playing a role in the ligand recognition function (46). These residues are all conserved across protozoan CYP51 and often phylum-specific (46). Thus, F48 (A' helix) is invariant across most biological kingdoms, but aligns with Y in all fungal CYP51 sequences. P210 (F'' helix) is conserved in protozoan, fungal, and plant CYP51, but corresponds to H in vertebrates. V213 (F'' helix) is conserved in protozoa and plants but aligns with F in fungi and W in vertebrates. F214 (F'' helix) is M or V in fungi, always L in vertebrates, and L or I in plants, while M460 (β4 hairpin) is only substituted with L in some filamentous fungi. These five residues contact the distal portion of the long arm of the VT-1161 molecule.

Fourteen other VT-1161-contacting residues line the inner surface of the CYP51 substrate binding cavity. Four residues are from the cytochrome P450 substrate recognition site 1 (SRS1) (47). Y103 and F110 (B' helix) are invariant in the whole family (>300 sequenced proteins), Y116 (B'' helix) is conserved in vertebrates, fungi, and protozoa yet replaced by F in all plants. In the ligand-free and sterol-bound protozoan CYP51 structures (3G1Q, (48) and 3P99 (49))

294 Y103 and Y116 form hydrogen bonds with the heme propionates, rings A and D, respectively.
295 Binding of some heme-coordinating ligands, however, was found to disrupt these H-bonds (32,
296 33, 36, 48, 50), which is likely to enhance the inhibitory potency of the compounds by
297 weakening the P450 heme support from the protein moiety (51). As it is seen in Figure 5B, in the
298 complex with *T. cruzi* CYP51 VT-1161 also disrupts the interaction between the heme and
299 Y116, by intercalating its β-phenyl ring between the bulky tyrosine side chain and the heme ring
300 D propionate. F110 contacts the β-phenyl ring of VT-1161 from the top. M106 (aligns with T in
301 fungal CYP51s) lies above the pyridine ring and two fluorine atoms of VT-1161. Six I-helix
302 residues (SRS4), A287, A288, F290, and A291, encircle the opposite side of the VT-1161 β-
303 phenyl ring, while G292 and T295 interact with the tetrazole ring. The remaining four VT-1161-
304 contacting residues (L356, L357, M358, and M360) are from SRS5 (K/β1-4 loop and β1-4
305 strand). They surround the two-ring area of the inhibitor.

306 The overall view of VT-1161 bound to *T. cruzi* CYP51 is shown in Figure 6. The phenoxy
307 arm of the inhibitor protrudes towards the distal surface of the protein and can be seen through
308 the entry into the substrate access channel (helices A', F'' and β4 hairpin) in the surface
309 representation model (Figure 6A, B). Such orientation is quite typical for CYP51 inhibitors
310 (Figure 6C), indicating that further elongation of the VT-1161 two ring arm is possible and may
311 well result in the compounds with even higher antiprotozoan activity. Moreover, crystallographic
312 analysis suggests (see also Table 2) that an elongation of this arm might also be favorable for
313 inhibition of *A. fumigatus*, as both CYP51 orthologs in this fungal pathogen have a flexible
314 methionine instead of bulky phenylalanine (F214) in this key position around the channel entry.
315 Respectively, the highest potency of VT-1161 to inhibit activity of *C. albicans* CYP51 (shown in
316 Figure 2) may be connected with the *C. albicans* F380 in the β1-4 strand (M360 in *T. cruzi*, M/L

in *A. fumigatus*) as in the *T. cruzi CYP51* co-structure this residue closely approaches the aromatic ring of VT-1161. Taking into account high structural similarity of CYP51 enzymes across phylogeny (29, 46), phenylalanine in this position is quite likely to form π–π stacking interactions with the inhibitor, thus significantly strengthening the VT-1161-*C. albicans* CYP51 complex. On the other side of the CYP51 binding cavity, the para-Cl atom in the β-phenyl ring of VT-1161 is directed towards A288. It is not excluded that a longer side chain of isoleucine (I304 in *C. albicans* CYP51) is more favorable here because it can form a larger number of van der Waals contacts with the inhibitor, while a leucine residue (L290/L304 in *A. fumigatus* CYP51A and B, respectively) might already be too bulky, creating some steric hindrances and therefore altering VT-1161 orientation.

DISCUSSION

Recent report demonstrated that a prospective, multicenter, randomized study called BENEFIT involving 2854 patients with Chagas' cardiomyopathy who received benznidazole or placebo (up to 80 days) and were followed for a mean of 5.4 years showed that although this drug largely decreased the detection of circulating parasites (by qPCR blood analysis), it was not able to reduce cardiac clinical progression (52), strengthening the need for alternative therapies for the millions of chagasic patients that are at the later disease stage (chronic phase).

Sterols are essential components of eukaryotic cells. They contribute to the stability, permeability, and fluidity of the membrane and participate in multiple regulatory processes, which are crucial for cell division, growth and multiplication. Therefore, the sterol biosynthetic pathway is highly conserved across biological kingdoms. Among all the enzymes involved in this pathway, inhibitors of the sterol 14α-demethylase (CYP51) are the most efficient antifungal

agents in clinical medicine and agriculture (18). Because the CYP51 orthologs appear to preserve their conserved biological function by maintaining high structural similarity of their substrate binding cavity at the secondary and tertiary levels (46), inhibitors of fungal CYP51 (such as the triazoles posaconazole and ravuconazole) are often also potent as inhibitors of the orthologous enzyme in protozoa, which makes drug repurposing possible and sometimes quite effective. In this study, we explored for the first time the antifungal clinical candidate 1-tetrazole VT-1161 as an inhibitor of CYP51 from the protozoan pathogen *T. cruzi* and found that the drug has strong potential as an antichagasic agent.

Historically, there has been relatively little variation in CYP51 inhibitor metal-binding groups (MBGs). First-generation antifungal drugs, such as miconazole and ketoconazole, utilized the 1-imidazole, a high-affinity ligand for heme-iron (53). These drugs also inhibited off-target human hepatic cytochrome P450 enzymes leading to severe and sometimes fatal liver problems (54). Second-generation azole antifungal drugs (e.g. itraconazole, voriconazole) utilized a 1,2,4-triazole. Compared to 1-imidazole, the 1,2,4-triazole was a lower-affinity ligand for heme-iron and this MBG alternative led to improved tolerability, but liver toxicity and drug-drug interactions remained problematic (26). VT-1161 was discovered using the strategy to investigate new, more selective agents focused on alternative, low-affinity MBG. In addition to its advantageous DMPK properties and excellent safety profile, VT-1161 is readily-prepared in seven synthetic transformations from available commercial reagents (21). Structural characterization of VT-1161 in complex with the target enzyme opens new opportunities for rational, structure directed design and optimization of new tetrazole-based CYP51 inhibitors.

In summary, our present findings demonstrate the potency of VT-1161 towards the *T. cruzi* CYP51 enzyme as well as its phenotypic efficacy against *T. cruzi* infection in *in vitro* and *in vivo*

biological assays, thus revealing a novel class of protozoan CYP51 inhibitors. A Chagas agent with robust pharmacokinetic characteristics has the potential to exhibit an improved profile within the CYP51 inhibitor class. The marked affinity of the 1-tetrazole example disclosed in detail in this paper, coupled with excellent *in vivo* exposure upon oral administration, could provide guidance toward discovery and development of novel and more efficient drug candidate(s) for the aforementioned neglected illness.

Financial support

This work was supported by Viamet Pharmaceuticals, Inc. (Durham, NC) and in part by National Institutes of Health Grant R01 GM067871 (to G.I.L.). Vanderbilt University is a member institution of the Life Science Collaborative Team (LS-CAT) at Sector 21 of the Advanced Photon Source (APS), Argonne, IL. Use of the APS at Argonne National Laboratory was supported by the United States Department of Energy, Office of Science, Office of Basic Energy Sciences, under Contract No. DE-AC02-06CH11357. Use of the LS-CAT Sector 21 was supported by the Michigan Economic Development Corporation and the Michigan Technology Tri-Corridor (Grant 085P1000817). The use of Confocal Microscopy Facility at Meharry was supported by MD007593 (F.V.). M.N.C.S. is research fellow of CNPq and CNE (FAPERJ).

REFERENCES

1. **Filardi LS, Brener Z.** 1987. Susceptibility and natural resistance of *Trypanosoma cruzi* strains to drugs used clinically in Chagas disease. Trans R Soc Trop Med Hyg **81:**755-759.

2. **Lepesheva GI.** 2013. Design or screening of drugs for the treatment of Chagas disease: what shows the most promise? Expert Opin Drug Discov **8:**1479-1489.

3. **WHO** (World Health Organisation). 2015. Third WHO report on neglected tropical diseases 2015: investing to overcome the global impact of neglected tropical diseases. WHO/HTM/NTD **2015.1**.

4. **Leslie M.** 2011. Drug developers finally take aim at a neglected disease. Science **333:**933-935.

5. **Esch KJ, Petersen CA.** 2013. Transmission and epidemiology of zoonotic protozoal diseases of companion animals. Clin Microbiol Rev **26:**58-85.

6. **Hotez PJ.** 2008. Neglected infections of poverty in the United States of America. PLoS Negl Trop Dis **2:**e256. doi:10.1371.

7. **Hotez P, Dumonteil E, Betancourt Cravioto M, Bottazzi M, Tapia-Conyer R.** 2013. An unfolding tragedy of Chagas disease in North America. PLoS Negl Trop Dis **7:**e2300. doi:2310.1371.

8. **Bern C, Kjos S, Yabsley MJ, Montgomery SP.** 2011. *Trypanosoma cruzi* and Chagas' disease in the United States. Clin Microbiol Rev **24:**655-681.

9. **Barry MA, Bezek S, Serpa JA, Hotez PJ, Woc-Colburn L.** 2012. Neglected infections of poverty in Texas and the rest of the United States: management and treatment options. Clin Pharmacol Ther **92:**170-181.

10. **Wilkinson SR, Taylor MC, Horn D, Kelly JM, Cheeseman I.** 2008. A mechanism for cross-resistance to nifurtimox and benznidazole in trypanosomes. Proc Natl Acad Sci U S A **105:**5022-5027.

11. **Maya JD, Cassels BK, Iturriaga-Vásquez P, Ferreira J, Faúndez M, Galanti N, Ferreira A, Morello A.** 2007. Mode of action of natural and synthetic drugs against *Trypanosoma cruzi* and their interaction with the mammalian host. Comp Biochem Physiol A: Mol Integr Physiol **146:**601-620.

12. **Papadopoulou MV, Bloomer WD, Lepesheva GI, Rosenzweig HS, Kaiser M, Aguilera-Venegas B, Wilkinson SR, Chatelain E, Ioset J-R.** 2015. Novel 3-nitrotriazole-based amides and carbinols as bifunctional antichagasic agents. J Med Chem **58:**1307-1319.

412 13. **Apt W.** 2010. Current and developing therapeutic agents in the treatment of Chagas disease.
413 Drug Design, Development and Therapy **4:**243-253.
414 14. **Clayton J.** 2010. Chagas disease: pushing through the pipeline. Nature **465:**S12-S15.
415 15. **Molina I, Salvador F, Sánchez-Montalvá A.** 2015. The use of posaconazole against Chagas
416 disease. Curr Opin Infect Dis **28:**397-407.
417 16. **Molina I, Gómez i Prat J, Salvador F, Treviño B, Sulleiro E, Serre N, Pou D, Roure S,**
418 **Cabezos J, Valerio L, Blanco-Grau A, Sánchez-Montalvá A, Vidal X, Pahissa A.** 2014.
419 Randomized trial of posaconazole and benznidazole for chronic Chagas' disease. N Engl J Med
420 **370:**1899-1908.
421 17. **Lepesheva GI, Waterman MR.** 2007. Sterol 14alpha-demethylase cytochrome P450 (CYP51), a
422 P450 in all biological kingdoms. Biochim Biophys Acta **1770:**467-477.
423 18. **Lepesheva GI, Villalta F, Waterman MR.** 2011. Targeting *Trypanosoma cruzi* sterol 14α-
424 demethylase (CYP51). Adv Parasitol **75:**65-87.
425 19. **Chatelain E, Konar N.** 2015. Translational challenges of animal models in Chagas disease drug
426 development: a review. Drug Design, Development and Therapy **9:**4807-4823.
427 20. **Denning DW, Bromley MJ.** 2015. How to bolster the antifungal pipeline. Science **347:**1414-
428 1416.
429 21. **Hoekstra WJ, Garvey EP, Moore WR, Rafferty SW, Yates CM, Schotzinger RJ.** 2014.
430 Design and optimization of highly-selective fungal CYP51 inhibitors. Bioorg Med Chem Lett
431 **24:**3455-3458.
432 22. **Warrilow AGS, Hull CM, Parker JE, Garvey EP, Hoekstra WJ, Moore WR, Schotzinger**
433 **RJ, Kelly DE, Kelly SL.** 2014. The clinical candidate VT-1161 is a highly potent inhibitor of
434 *Candida albicans* CYP51 but fails to bind the human enzyme. Antimicrob Agents Chemother
435 **58:**7121-7127.

23. **Garvey EP, Hoekstra WJ, Moore WR, Schotzinger RJ, Long L, Ghannoum MA.** 2015. VT-1161 Dosed once daily or once weekly exhibits potent efficacy in treatment of dermatophytosis in a guinea pig model. Antimicrob Agents Chemother **59:**1992-1997.

24. **Garvey EP, Hoekstra WJ, Schotzinger RJ, Sobel JD, Lilly EA, Fidel PL.** 2015. Efficacy of the clinical agent VT-1161 against fluconazole-sensitive and -resistant *Candida albicans* in a murine model of vaginal candidiasis. Antimicrob Agents Chemother **59:**5567-5573.

25. **Shubitz LF, Trinh HT, Galgiani JN, Lewis ML, Fothergill AW, Wiederhold NP, Barker BM, Lewis ERG, Doyle AL, Hoekstra WJ, Schotzinger RJ, Garvey EP.** 2015. Evaluation of VT-1161 for treatment of coccidioidomycosis in murine infection models. Antimicrob Agents Chemother. Sep 14. pii: AAC.00593-15.

26. **Pitman SK, Drew RH, Perfect JR.** 2011. Addressing current medical needs in invasive fungal infection prevention and treatment with new antifungal agents, strategies and formulations. Expert Opin Emerg Drugs **16:**559-586.

27. **Lepesheva GI, Zaitseva NG, Nes WD, Zhou W, Arase M, Liu J, Hill GC, Waterman MR.** 2006. CYP51 from *Trypanosoma cruzi*: a phyla-specific residue in the B' helix defines substrate preferences of sterol 14alpha-demethylase. J Biol Chem **281:**3577-3585.

28. **Lepesheva GI, Podust LM, Bellamine A, Waterman MR.** 2001. Folding requirements are different between sterol 14α-demethylase (CYP51) from *Mycobacterium tuberculosis* and human or fungal orthologs. J Biol Chem **276:**28413-28420.

29. **Hargrove TY, Wawrzak Z, Lamb DC, Guengerich FP, Lepesheva GI.** 2015. Structure-functional characterization of cytochrome P450 sterol 14α-demethylase (CYP51B) from *Aspergillus fumigatus* and molecular basis for the development of antifungal drugs. J Biol Chem **290**:23916-23934.

30. **Lepesheva GI, Nes WD, Zhou W, Hill GC, Waterman MR.** 2004. CYP51 from *Trypanosoma brucei* is obtusifoliol-specific. Biochemistry **43:**10789-10799.

31. **Lepesheva GI, Ott RD, Hargrove TY, Kleshchenko YY, Schuster I, Nes WD, Hill GC, Villalta F, Waterman MR.** 2007. Sterol 14 alpha-demethylase as a potential target for antitrypanosomal therapy: enzyme inhibition and parasite cell growth. Chem Biol **14:**1283-1293.

32. **Lepesheva GI, Hargrove TY, Anderson S, Kleshchenko Y, Furtak V, Wawrzak Z, Villalta F, Waterman MR.** 2010. Structural insights into inhibition of sterol 14 alpha-demethylase in the human pathogen *Trypanosoma cruzi*. J Biol Chem **285:**25582-25590.

33. **Hargrove TY, Wawrzak Z, Alexander PW, Chaplin JH, Keenan M, Charman SA, Waterman MR, Chatelain E, Lepesheva GI.** 2013. Complexes of *Trypanosoma cruzi* sterol 14α-demethylase (CYP51) with two pyridine-based drug candidates for Chagas disease: structural basis for pathogen selectivity. J Biol Chem **288:**31602-31615.

34. **Omura T, Sato R.** 1964. The carbon monoxide-binding pigment of liver microsomes. I. Evidence for Its hemoprotein nature. J Biol Chem **239:**2370-2378.

35. **Schenkman JB, Remmer H, Estabrook RW.** 1967. Spectral studies of drug interaction with hepatic microsomal cytochrome. Mol Pharmacol **3:**113-123.

36. **Friggeri L, Hargrove TY, Rachakonda G, Williams AD, Wawrzak Z, Di Santo R, De Vita D, Waterman MR, Tortorella S, Villalta F, Lepesheva GI.** 2014. Structural basis for rational design of inhibitors targeting *Trypanosoma cruzi* sterol 14α-demethylase: two regions of the enzyme molecule potentiate its inhibition. J Med Chem **57:**6704-6717.

37. **Lima MF, Villalta F.** 1989. *Trypanosoma cruzi* trypomastigote clones differentially express a parasite cell adhesion molecule. Mol Biochem Parasitol **33:**159-170.

38. **Villalta F, Dobish MC, Nde PN, Kleshchenko YY, Hargrove TY, Johnson CA, Waterman MR, Johnston JN, Lepesheva GI.** 2013. VNI cures acute and chronic experimental Chagas disease. J Infect Dis **208:**504-511.

39. **Johnson CA, Rachakonda G, Kleshchenko YY, Nde PN, Madison MN, Pratap S, Cardenas TC, Taylor C, Lima MF, Villalta F.** 2013. Cellular response to *Trypanosoma cruzi* infection

induces secretion of defensin α-1, which damages the flagellum, neutralizes trypanosome motility, and inhibits infection. Infect Immun **81:**4139-4148.

40. **Collaborative Computational Project N.** 1994. The CCP4 suite: programs for protein crystallography. Acta Crystallogr D Biol Crystallogr **50:**760-763.

41. **Emsley P, Lohkamp B, Scott WG, Cowtan K.** 2010. Features and development of Coot. Acta Crystallogr D Biol Crystallogr **66:**486-501.

42. **Cencig S, Coltel N, Truyens C, Carlier Y.** 2012. Evaluation of benznidazole treatment combined with nifurtimox, posaconazole or AmBisome® in mice infected with *Trypanosoma cruzi* strains. Int J Antimicrob Agents **40:**527-532.

43. **Buckner F, Bahia MT, Suryadevara PK, White KL, Shackleford DM, Chennamaneni NK, Hulverson MA, Laydbak JU, Chatelain E, Scandale I, Verlinde CL, Charman SA, Lepesheva GI, Gelb MH** 2012. Pharmacological characterization, structural studies, and in vivo activity of anti-Chagas disease lead compounds derived from tipifarnib. Antimicrob Agents Chemother **56:**4914-4921.

44. **Soeiro MdNC, de Souza EM, da Silva CF, Batista DdGJ, Batista MM, Pavão BP, Araújo JS, Lionel J, Britto C, Kim K, Sulikowski G, Hargrove TY, Waterman MR, Lepesheva GI.** 2013. *In vitro* and *in vivo* studies of the antiparasitic activity of sterol 14α-demethylase (CYP51) inhibitor VNI against drug-resistant strains of *Trypanosoma cruzi*. Antimicrob Agents Chemother **57:**4151-4163.

45. **Cherkesova TS, Hargrove TY, Vanrell MC, Ges I, Usanov SA, Romano PS, Lepesheva GI.** 2014. Sequence variation in CYP51A from the Y strain of *Trypanosoma cruzi* alters its sensitivity to inhibition. FEBS Lett **588:**3878-3885.

46. **Lepesheva GI, Waterman MR.** 2011. Structural basis for conservation in the CYP51 family. Biochim Biophys Acta **1814:**88-93.

47. **Gotoh O.** 1992. Substrate recognition sites in cytochrome P450 family 2 (CYP2) proteins inferred from comparative analyses of amino acid and coding nucleotide sequences. J Biol Chem **267:**83-90.

48. **Lepesheva GI, Park HW, Hargrove TY, Vanhollebeke B, Wawrzak Z, Harp JM, Sundaramoorthy M, Nes WD, Pays E, Chaudhuri M, Villalta F, Waterman MR.** 2010. Crystal structures of *Trypanosoma brucei* sterol 14 alpha-demethylase and implications for selective treatment of human infections. J Biol Chem **285:**1773-1780.

49. **Hargrove TY, Wawrzak Z, Liu J, Waterman MR, Nes WD, Lepesheva GI.** 2012. Structural complex of sterol 14α-demethylase (CYP51) with 14α-methylenecyclopropyl-Δ7-24, 25-dihydrolanosterol. J Lipid Res **53:**311-320.

50. **Hargrove TY, Wawrzak Z, Liu J, Nes WD, Waterman MR, Lepesheva GI.** 2011. Substrate preferences and catalytic parameters determined by structural characteristics of sterol 14α-demethylase (CYP51) from *Leishmania infantum*. J Biol Chem **286:**26838-26848.

51. **Lepesheva GI, Waterman MR.** 2011. Sterol 14alpha-demethylase (CYP51) as a therapeutic target for human trypanosomiasis and leishmaniasis. Curr Top Med Chem **11** 2060-2071.

52. **Morillo CA, Marin-Neto JA, Avezum A, Sosa-Estani S, Rassi A, Rosas F, Villena E, Quiroz R, Bonilla R, Britto C, Guhl F, Velazquez E, Bonilla L, Meeks B, Rao-Melacini P, Pogue J, Mattos A, Lazdins J, Connolly SJ, Yusuf S.** 2015. Randomized trial of benznidazole for chronic Chagas' cardiomyopathy. N Eng J Med **373**:1295-306.

53. **Heeres J, Meerpoel L, Lewi P.** 2010. Conazoles. Molecules **15:**4129-4188.

54. **Lewis RE.** 2011. Current concepts in antifungal pharmacology. Mayo Clin Proc **86:**805-817.

533 **FIGURE LEGENDS**

534 **Figure 1. Spectral response of (A) *T. cruzi* CYP51 to the addition of the heme-coordinating**
535 **ligand 1-tetrazole VT-1161**, shown as the difference type 2 binding spectra. The P450
536 concentration was 0.3 µM, and the optical path length was 5 cm. The titration curve obtained
537 using equation 1 is presented in the inset. **B**. The corresponding titration curves and type 2
538 spectral responses of *A. fumigatus* (upper) and *C. albicans* (lower) CYP51 orthologs.

539 **Figure 2. Inhibitory effects of VT-1161 on the enzymatic activities of sterol 14α-**
540 **demethylases from the protozoan parasite *T. cruzi* and the opportunistic fungal pathogens**
541 ***C. albicans* and *A. fumigatus*.** The incubation time was 60 min. The molar
542 enzyme/inhibitor/substrate (E/I/S) ratio was 1:2:50. The experiments were performed in
543 triplicate, and results are presented as means ± standard error (SE).

544 **Figure 3. Cellular effects of VT1161 in Tulahuen *T. cruzi* infected cardiomyocytes.**
545 Cardiomyocyte monolayers were exposed to green fluorescent protein–expressing
546 trypomastigotes (10 parasites per cell) for 24 hours and then treated with VT-1161 or with the
547 corresponding volumes of DMSO. Fluorescence microscopic observations of *T. cruzi* inside
548 cardiomyocytes treated with DMSO (control) (**A**) or with 10 (**B**) and 25 (**C**) nM of VT-1161, 72
549 hours after infection. *T. cruzi* amastigotes are green, cardiomyocyte nuclei are blue, and
550 cardiomyocyte actin myofibrils are red. **D.** Dose-dependent clearance of the parasite. The
551 infection was quantified by determining the fluorescence, indicated as relative fluorescence units
552 (RFU) at 72 hours. The experiments were performed in triplicate, and results are presented as
553 means ± SE.

554 **Figure 4. VT-1161 suppresses parasitemia in mice infected with *T. cruzi*.** Groups of Swiss
555 female mice (n=6) were i.p. infected with 10^4 blood trypomastigotes of the Y strain of *T. cruzi*

and non-treated (control), or treated with 0.5% carboxymethylcellulose (vehicle) or 50 mg/kg of VT-1161. The treatment was started on day 5 after infection and performed by oral gavage. The bars represent mean ± SE. Three days of treatment with VT-1161 caused >99.8% suppression of parasitemia.

Figure 5. **A.** Structural formula (top) and the 2Fo-Fc electron density map (bottom) of VT-1161 coordinated to the *T. cruzi* CYP51 heme iron. Here and in Fig. 6 VT-1161 is presented as a stick model, the carbon atoms are green. The map is shown as grey mesh and contoured at 1.3 sigma. The heme is depicted as a wire model, the carbon atoms are grey. **B**. Nineteen amino acid residues that surround VT-1161 in the *T. cruzi* CYP51 active site. The corresponding secondary structural elements of the enzyme are presented as semitransparent ribbons and marked. (The corresponding residues in the aligned sequences of CYP51 from *C. albicans* and *A. fumigatus* are listed in Table 2).

Figure 6. VT-1161 (shown as a stick model with green carbon atoms) bound to *T. cruzi* CYP51. **A**. Overall view; the protein backbone is depicted as a rainbow ribbon colored by secondary structure succession from blue (N-terminus) to red (C-terminus). A surface representation is shown alongside to outline the view of VT-1161 through the entrance into the enzyme substrate access channel.**B**. A slice through the protein surface showing the location of VT-1161 within the CYP51 active site cavity. The orientation is about the same as in **A**; enlarged view. **C**. Superimposition of VT-1161 with imidazole LFD (blue), triazole posaconazole (khaki), and pyridine UDO (yellow) in the *T. cruzi* CYP51 active site, PDB IDs of the corresponding structures are 4CK8, 3K1O, and 3ZG2, respectively.

Table 1. Data collection and refinement statistics.

Complex	*T. cruzi* CYP51-VT-1161 (ligand PDB ID VT1)
Data collection	
Wavelength, Å	0.9786
Cell dimensions	
a, b, c, Å	63.06; 63.06; 221.75
α, β, γ, °	90.00, 90.00, 120.00
Molecules per asymmetric unit	1
Solvent content, %	47.8
Resolution (outer shell), Å	54.6-2.75 (2.82-2.75)
Number of reflections (outer shell)	14063 (1526)
R_{merge} (outer shell)	0.065 (0.695)
I/σ (outer shell)	23.1 (2.7)
Completeness (outer shell), %	99.8 (100)
Redundancy (outer shell)	8.0 (4.6)
Refinement	
R-work	0.259
R-free	0.270
Rms deviations from ideal geometry	
Bond lengths, Å	0.002
Bond angles, °	0.89
Ramachandran plot	
Residues in favorable/allowed regions (%)	96.4/99.8
Outliers (%)	0.2
Number of atoms (mean B-factor, Å)	3672 (118.5)
Number of residues	
Protein (mean B-factor, Å)	450 (120.7)
Heme (mean B-factor, Å)	1 (76.4)
Ligand (mean B-factor, Å)	VT1 1 (99.6)
PDB code	5AJR

Table 2. VT-1161 contacting residues in *T. cruzi* CYP51 and the corresponding residues in the aligned CYP51 orthologs from two opportunistic fungal pathogens, *C. albicans* (yeast) and *A. fumigatus* (filamentous fungus; *A. fumigatus* has two CYP51 genes, A and B (24)).

Secondary structural element	*T. cruzi*	*C. albicans*	*A. fumigatus*	
			A	B
A' helix	F48	Y64	Y53	Y68
B' helix	Y103 M106 F110	Y118 T122 F126	Y107 T111 F115	Y122 T126 F130
B'C loop	Y116	Y132	Y121	Y136
F'' helix	P210 V213 F214	P230 F233 V234	P216 F219 **M220**	P231 F234 **M235**
I helix	A287 A288 F290 A291 G292 T295	G303 **I304** M306 G307 G308 T311	T289 L290 M292 A293 G294 S297	A303 L304 M306 A307 G308 S311
K/β1-4 loop	L356 L357 M358	L376 H377 S378	I364 H365 S366	I373 H374 S375
β1-4 strand	M360	**F380**	M368	I377
β4 hairpin	M460	M508	L494	L503

Figure 1

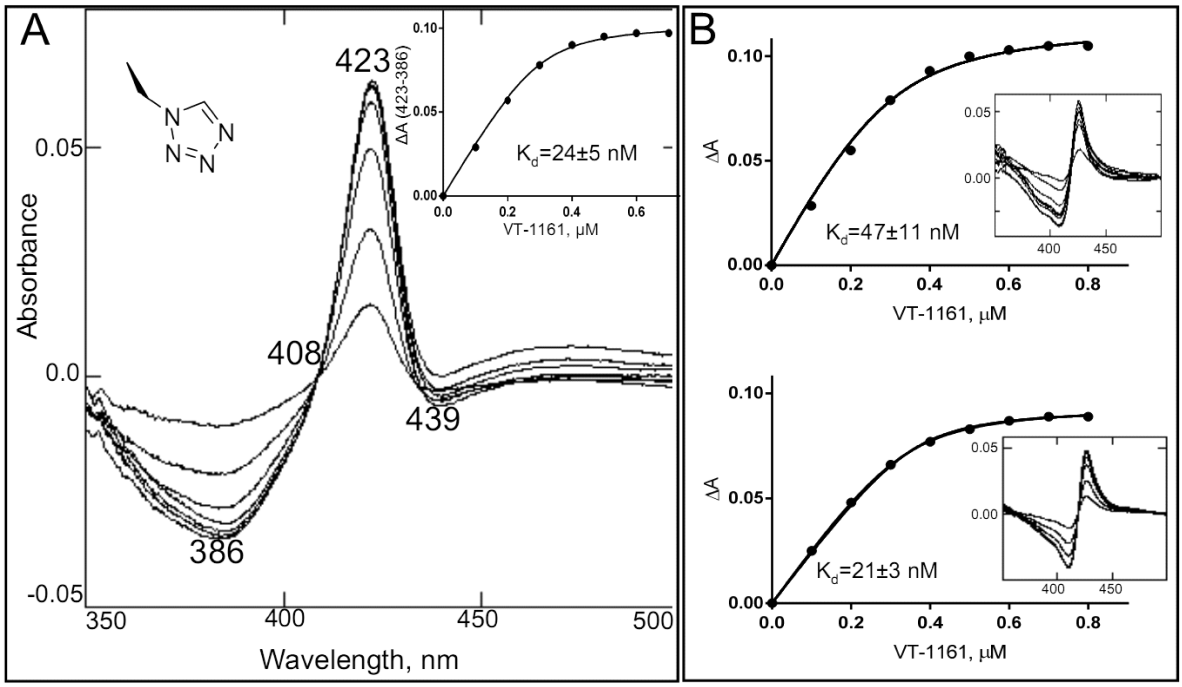

Figure 2

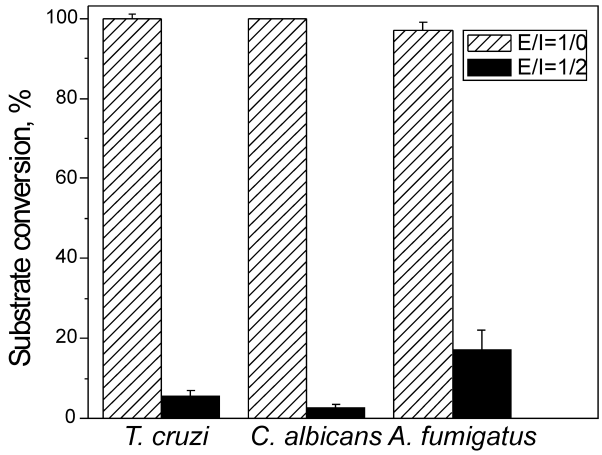

Figure 3

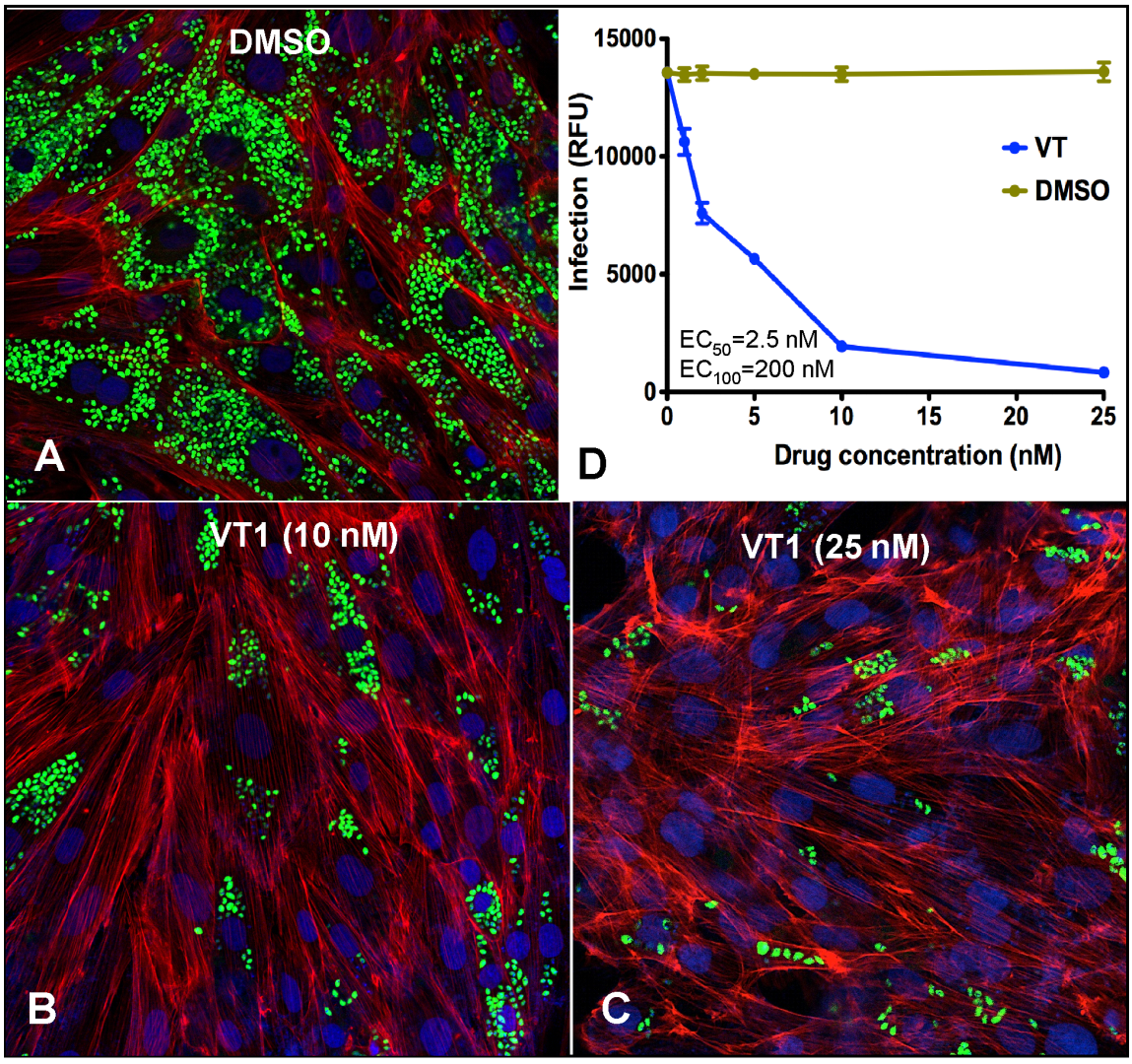

Figure 4

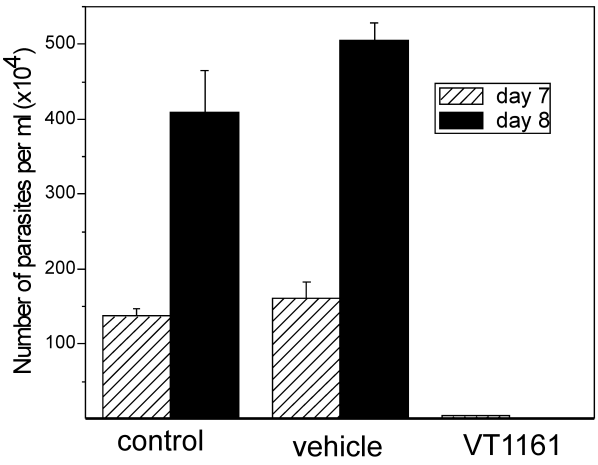

Figure 5

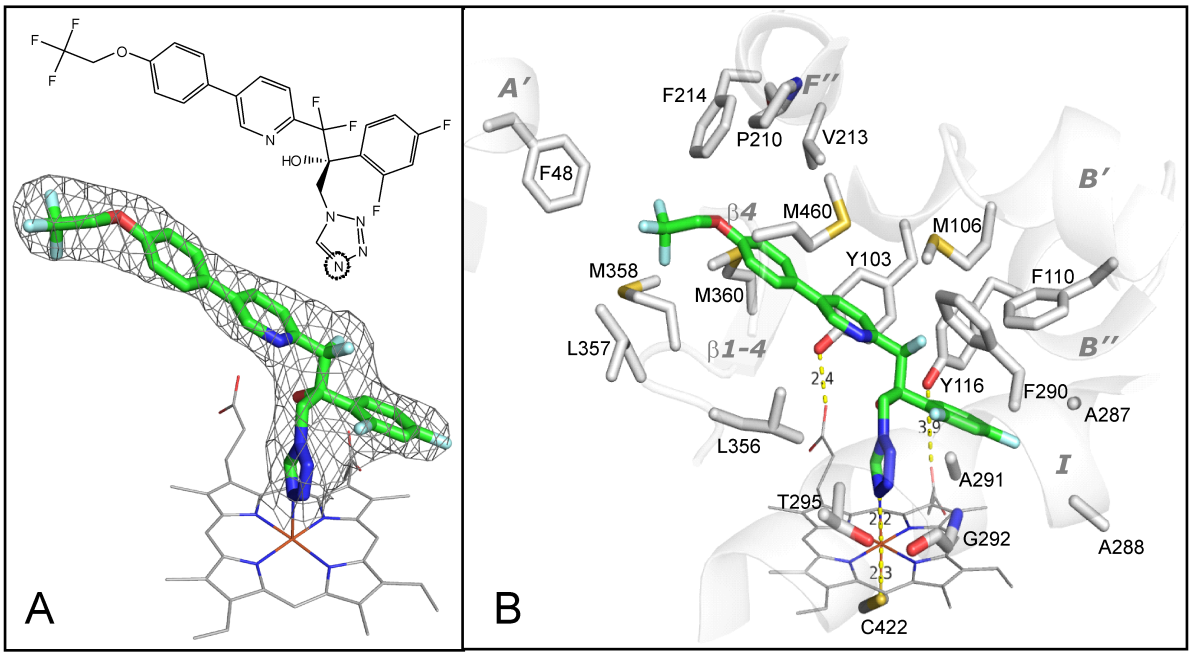

Figure 6